Application of Cauchy-type integrals in developing effective methods for depth-to-basement inversion of gravity and gravity gradiometry data

Hongzhu Cai[1] and Michael Zhdanov[2]

ABSTRACT

One of the most important applications of gravity surveys in regional geophysical studies is determining the depth to basement. Conventional methods of solving this problem are based on the spectrum and/or Euler deconvolution analysis of the gravity field and on parameterization of the earth's subsurface into prismatic cells. We have developed a new method of solving this problem based on 3D Cauchy-type integral representation of the potential fields. Traditionally, potential fields have been calculated using volume integrals over the domains occupied by anomalous masses subdivided into prismatic cells. This discretization can be computationally expensive, especially in a 3D case. The technique of Cauchy-type integrals made it possible to represent the gravity field and its gradients as surface integrals. In this approach, only the density contrast surface between sediment and basement needed to be discretized for the calculation of gravity field. This was especially significant in the modeling and inversion of gravity data for determining the depth to the basement. Another important result was developing a novel method of inversion of gravity data to recover the depth to basement, based on the 3D Cauchy-type integral representation. Our numerical studies determined that the new method is much faster than conventional volume discretization method to compute the gravity response. Our synthetic model studies also showed that the developed inversion algorithm based on Cauchy-type integral is capable of recovering the geometry and depth of the sedimentary basin effectively with a complex density profile in the vertical direction.

INTRODUCTION

There is strong interest in developing effective methods of inverting gravity data for depth-to-basement and density contrast estimation. Many research papers have been published over the past decade on this subject (e.g., Barbosa et al., 1997, 1999a, 1999b; Silva et al., 2001, 2006, 2007, 2010a, 2010b; Gallardo-Delgado et al., 2003; Martins et al., 2010, 2011a, 2011b). The conventional approach to solving depth-to-basement gravity inverse problems is based on parameterization of the earth's subsurface, containing the sedimentary pack, into prismatic cells with known horizontal dimensions and known density contrast, and on estimation of the cell's thicknesses. We present a novel approach to the solution of this problem based on 3D analogs of Cauchy-type integrals, introduced by Zhdanov (1980, 1984, 1988). These integrals extend to the 3D case all the major properties of classical Cauchy integrals of the theory of functions of complex variables. In a 2D case, Cauchy integrals can be used to provide an effective representation of the gravity field of 2D density distributions and to solve the problems of the upward and downward analytic continuation of the potential field data. It was demonstrated in papers by Zhdanov (1980) that 3D analogs of Cauchy-type integrals make it possible to extend a large body of the research developed for 2D potential fields into 3D cases. For example, in the paper by Zhdanov and Liu (2013), 3D Cauchy-type integrals are applied for solving the problem of terrain correction for gravity and gravity gradiometry data. In the paper by Zhdanov and Cai (2013), the authors apply 3D Cauchy-type integrals to modeling and inversion of gravity fields caused by

sediment-basement interface with constant density contrast. Cai and Zhdanov (2015) introduce the method of inverting magnetic field data to recover the depth to basement using Cauchy-type integrals.

In the present paper, we apply the method of 3D Cauchy-type integrals to solving forward and inverse problems for a density contrast model. This type of models is used, for example, in the inversion of the gravity data for the depth to basement. In our study, we consider a model formed by two quasihorizontal layers, the upper layer representing the sediments and the lower layer describing the basement. We assume that the density does not vary in the horizontal direction, but, in a general case, it may vary vertically, having a discontinuity at the surface of the basement. The goal is to find the surface of the basement, which is a density contrast surface in this case.

We develop an inversion scheme to determine the density contrast surface. Gravity field and/or full-tensor gravity gradiometry data can be used for the inversion. The inversion scheme is based on the reweighted regularized conjugate gradient method (Zhdanov, 2002). Note that the method based on the Cauchy-type integrals requires the discretization of the contrast surface only, which reduces dramatically the computing resources in comparison with the conventional methods based on volume discretization into prismatic cells.

The conventional methods of solving this problem are based on the spectrum and/or Euler deconvolution analysis of the gravity field. However, these methods have several limitations. In the framework of the spectrum method, the gravity field needs to be analyzed within a moving window and the size of the window needs to be determined based on an expected depth to the source, which is usually either unavailable or not accurate (Chávez et al., 1999). A complex source structure can complicate the spectrum analysis, which may result in significant errors of the depth estimation (Odegard, 2011). The conventional Euler deconvolution method can be used for fast depth estimation, but it requires the input of the source structure index to estimate the depth to the source, which simplifies the source to some specific geometries, such as sphere, cylinder, etc. (Lafehr and Nabighian, 2012). Even though an extended Euler deconvolution method can be used to estimate the source depth and the structure index simultaneously, it is still difficult to deal with a complex source structure (Lafehr and Nabighian, 2012). Moreover, the spectrum and Euler deconvolution methods do not provide a direct comparison between the observed and predicted gravity field data, which makes it difficult to evaluate the correctness of the solution for the depth to basement. In comparison with those methods, our method is based on direct evaluation of the misfit between the observed and predicted data. In addition, as we will see below, the a priori information can also be incorporated into the inversion in the framework of the method based on the Cauchy-type integrals.

The developed method was tested for inversion of the gravity data computer simulated for typical contrast surface models. We also apply this method to field gravity data in the Big Bear Lake area in California to recover the depth to the basement.

CAUCHY-TYPE REPRESENTATION OF A GRAVITY FIELD CAUSED BY A 3D BODY

The gravity field at location $\mathbf{r}'$ (outside the source) caused by a 3D body with constant density ρ_0 can be calculated by the following equation:

$$\mathbf{g}(\mathbf{r}') = -G \int \int \int_D \rho_0 \nabla \frac{1}{|\mathbf{r} - \mathbf{r}'|} dv, \qquad (1)$$

where G is the universal gravitational constant, D is the domain filled by constant density ρ_0, and radius vectors $\mathbf{r}'$ and $\mathbf{r}$ denote the locations of the points of observation and integration, respectively.

For complex geometry, this integral needs to be evaluated numerically. The common approach is to discretize the volume into a grid of prisms. This method can be computationally expensive for large-scale modeling and inversion.

It is shown by Zhdanov (1988) and Zhdanov and Liu (2013) that the gravity field caused by a 3D body D with surface S and a constant density can be expressed as follows:

$$\mathbf{g}(\mathbf{r}') = \frac{4\pi G\rho_0}{3} [\mathbf{C}^s(\mathbf{r}', \mathbf{r}) - \mathbf{C}^s(\mathbf{r}', \mathbf{r}')]$$
$$= \frac{4\pi}{3} G\rho_0 \mathbf{C}^s(\mathbf{r}', \mathbf{r} - \mathbf{r}'), \qquad (2)$$

where 3D analog of the Cauchy-type integral $\mathbf{C}^s$ was introduced by Zhdanov (1988) as follows:

$$\mathbf{C}^s(\mathbf{r}', \boldsymbol{\varphi}) = \frac{-1}{4\pi} \int \int_S \left[(\mathbf{n} \times \boldsymbol{\varphi}) \nabla \frac{1}{|\mathbf{r} - \mathbf{r}'|} + (\mathbf{n} \times \boldsymbol{\varphi}) \right.$$
$$\left. \times \nabla \frac{1}{|\mathbf{r} - \mathbf{r}'|} \right] ds. \qquad (3)$$

For completeness, the definition and major properties of the Cauchy-type integral are given in Appendix A.

The previous equation can be rewritten in a matrix notation for the scalar components of the gravity field as follows:

$$g_\alpha = -\frac{G\rho_0}{3} \int \int_S \Delta_{\alpha\beta\gamma\eta} \frac{(r_\beta - r'_\beta)(r_\eta - r'_\eta)}{|\mathbf{r} - \mathbf{r}'|^3} n_\gamma ds,$$
$$\alpha, \beta, \gamma, \eta = x, y, z, \qquad (4)$$

where the four-index Δ-symbol is expressed in terms of the symmetric Kronecker symbol $\delta_{\alpha\beta}$ as

$$\Delta_{\alpha\beta\gamma\eta} = \delta_{\alpha\beta}\delta_{\gamma\eta} + \delta_{\alpha\eta}\delta_{\beta\gamma} - \delta_{\alpha\gamma}\delta_{\beta\eta}; \delta_{\alpha\beta} == \begin{cases} 1, & \alpha = \beta \\ 0, & \alpha \neq \beta \end{cases}, \qquad (5)$$

and all the notations are described in Appendix A.

We can use equation 4 to calculate the gravity gradient tensor whose scalar components are equal to the derivatives of the corresponding scalar components of the gravity field with respect to the spatial coordinates:

$$g_{\alpha v} = \frac{\partial g_\alpha}{\partial v'}, \qquad \alpha, v = x, y, z. \qquad (6)$$

After some algebra, one can express equation 6 in a matrix notation as follows:

$$g_{\alpha v}(\mathbf{r}') = G\rho_0 \int\int_S \frac{\Delta_{\alpha\beta\gamma\eta}r_\beta}{|\mathbf{r}-\mathbf{r}'|^5}[3(r_v - r_v')(r_\eta - r_\eta')$$
$$- |\mathbf{r}-\mathbf{r}'|^2\delta_{v\eta}]n_\gamma \mathrm{d}s. \tag{7}$$

From equations 4 and 7, we can see that the gravity field caused by a volume D filled by masses with some constant density ρ_0 can be represented as the Cauchy-type integral over the surface S of the volume. Thus, the original formula for calculating the gravity field as a volume integral is reduced to the surface integral.

It is also important to point out that the density distribution inside volume D may not necessarily be a constant value. It is shown by Zhdanov (1988) and Zhdanov and Liu (2013) that one can incorporate arbitrary analytic density-depth distribution within the volume in this formula. The advantage is that in applications, we can use this method to simulate the potential field due to the sedimentary basin, which is usually characterized by the density change with depth.

CAUCHY-TYPE REPRESENTATION OF THE GRAVITY FIELD AND ITS GRADIENT FOR A DENSITY CONTRAST SURFACE

Let us consider a model of the sediment-basement interface with a density contrast at some surface Γ, shown in Figure 1. We assume that surface Γ is described by equation $z = h(x, y) - H_0$, and a horizontal plane P is given by equation $z = -H_0$ with

$$H_0 \geq h(x, y) \geq 0 \tag{8}$$

and

$$h(x, y) - H_0 \to 0 \quad \text{for} \sqrt{x^2 + y^2} \to \infty, \tag{9}$$

where H_0 is a constant. Let us draw a sphere O_R of radius R with the center in the origin of the Cartesian system of coordinates. We de-

note by Γ_R and P_R the parts of the surfaces Γ and P, respectively, located within the sphere O_R. For the first model, we assume that the real sediment-basement interface Γ_R is located above plane P. We also assume that the sediment layer has a constant density ρ_s and the basement has a constant density ρ_b ($\rho_b > \rho_s$). We also assume that Γ and P extend infinitely in the horizontal direction and $\Gamma_R \to P$ at infinity. The gravity anomaly is caused by the density volume D_R, which is bounded by a closed surface, formed by Γ_R and P_R and the parts of the sphere O_R between these two surfaces as shown in Figure 1.

It is demonstrated by Zhdanov (1988) that the gravity field caused by volume D_R is expressed by

$$\mathbf{g}(\mathbf{r}') = 4\pi G\rho_0\mathbf{C}^{\Gamma_R}(\mathbf{r}', (z + H_0)\mathbf{d}_z), \tag{10}$$

in the case where $\Gamma_{R\to\infty} \to P$ at infinity. As a result, the Cauchy-type integral in equation 10 is calculated along an infinitely extended surface Γ.

In equation 10, ρ_0 is the density contrast between the sediments and the basement:

$$\rho_0 = \rho_b - \rho_s > 0. \tag{11}$$

For the model shown in Figure 1, we always have a positive gravity anomaly. Now, we consider another model presented in Figure 2, in which the density contrast surface is below the horizontal plane P. In this case, we have a negative density anomaly caused by the deficit of masses located within domain D_R.

Similarly, the gravity field can be expressed as

$$\mathbf{g}(\mathbf{r}') = 4\pi G(-\rho_0)\mathbf{C}^{\Gamma_R}(\mathbf{r}', (z + H_0)\mathbf{d}_z). \tag{12}$$

We have the following expressions for the scalar components of the normal vector pointing outside domain D_R for a model shown in Figure 1:
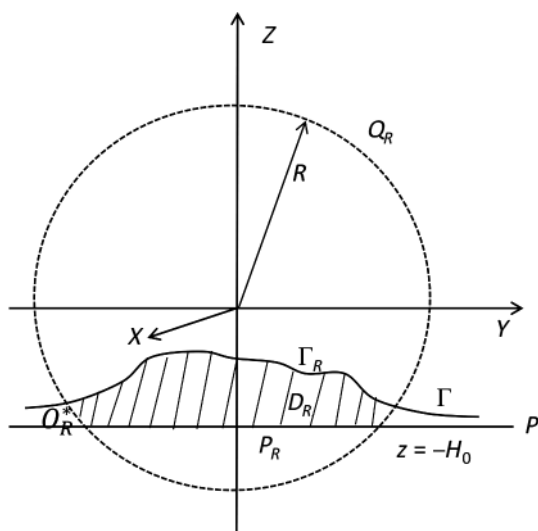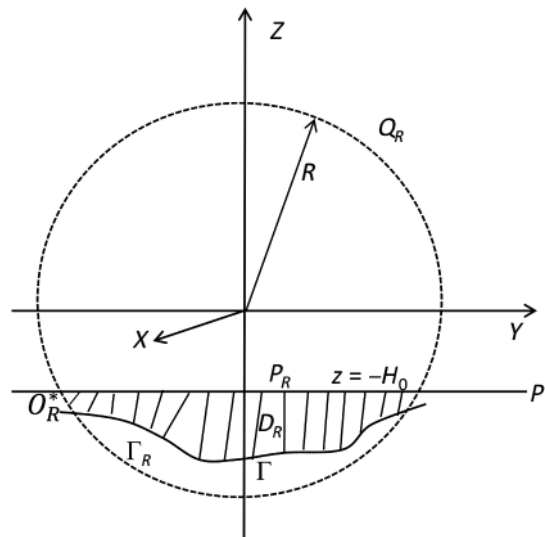

Figure 1. Density contrast model for a sediment-basement interface with a positive anomaly. The horizontal plane P is located at the average depth of the sediment-basement interface, and Γ_R is the actual sediment-basement interface.

Figure 2. Density contrast model for a sediment-basement interface with a negative anomaly. The horizontal plane P is located at the average depth of the sediment-basement interface, and Γ_R is the actual sediment-basement interface.

$$n_x ds = -\frac{\partial h(x,y)}{\partial x} dxdy = b_x(x,y)dxdy,$$

$$n_y ds = -\frac{\partial h(x,y)}{\partial y} dxdy = b_y(x,y)dxdy, \text{ and } n_z ds$$

$$= dxdy = b_z(x,y)dxdy, \tag{13}$$

where

$$b_x(x,y) = -\frac{\partial h(x,y)}{\partial x}, \quad b_y(x,y) = -\frac{\partial h(x,y)}{\partial y},$$

$$b_z(x,y) = 1, \quad h = z + H_0. \tag{14}$$

Similarly, for the model shown in Figure 2, the scalar components of the normal vector pointing outside domain D_R are equal to the following equations:

$$n_x ds = \frac{\partial h(x,y)}{\partial x} dxdy = -b_x(x,y)dxdy,$$

$$n_y ds = \frac{\partial h(x,y)}{\partial y} dxdy = -b_y(x,y)dxdy, \text{ and } n_z ds$$

$$= -dxdy = -b_z(x,y)dxdy. \tag{15}$$

It is important to note that, although for the models in Figures 1 and 2, the equations for the normal vector have a different sign, as shown in equations 13 and 15, respectively, the final expressions for the fields are exactly the same because the signs for the anomalous densities for models 1 and 2 are also different. Thus, in matrix notations, the gravity field caused by the density anomaly for model 1 (Figure 1) and model 2 (Figure 2) can be expressed using a unified equation as follows:

$$g_\alpha(\mathbf{r}') = -G\rho_0 \int \int_S \Delta_{\alpha z \gamma \eta} \frac{h(x,y)(r_\eta - r_\eta')}{|\mathbf{r} - \mathbf{r}'|^3} b_\gamma dxdy, \tag{16}$$

$$\alpha, \gamma, \eta = x, y, z.$$

Similarly, the gravity gradient for the models in Figures 1 and 2 can also be unified as

$$g_{\alpha v}(\mathbf{r}') = -G\rho_0 \int \int_S \frac{\Delta_{\alpha z \gamma \eta} h(x,y)}{|\mathbf{r} - \mathbf{r}'|^5} [3(r_v - r_v')(r_\eta - r_\eta')$$

$$- |\mathbf{r} - \mathbf{r}'|^2 \delta_{v\eta}] b_\gamma dxdy, \tag{17}$$

where $\alpha, \gamma, \eta = x, y, z$.

As we mentioned above, in a general case, the density contrast value is a function of depth:

$$\Delta\rho = f(z). \tag{18}$$

In this case, the representation of the gravity field caused by the sediment-basement interface takes the following form (Zhdanov, 1988; Zhdanov and Liu, 2013):

$$\mathbf{g}(\mathbf{r}') = 4\pi G \mathbf{C}^{\Gamma_R}(\mathbf{r}', [R(\mathbf{z}) - R(-H_0)]\mathbf{d}_z), \tag{19}$$

where

$$R(\mathbf{z}) = \int_{-H_0}^z f(z)dz. \tag{20}$$

Similar equations can be derived for the gravity gradient component by taking the spatial derivative of the forward operator for the gravity field.

Equations 16 and 17 represent the gravity and gravity gradient fields in the form of Cauchy-type integrals over the density contrast surface corresponding to the sediment-basement interface. These expressions provide an analytic basis for a fast method of numerical modeling of gravity and gravity gradiometry data. Both of these two equations need to be discretized to be solved numerically. In the paper by Zhdanov and Liu (2013), rectangular and triangular discretizations of the density contrast surface are introduced. Numerically, rectangular is simpler than triangular discretization. However, triangular discretization is demonstrated to have higher accuracy than rectangular. In our forward modeling part, both of these two types of discretization are implemented. In the inversion part, only the rectangular discretization is used for simplicity.

In particular, we can approximate the density contrast surface within each cell k by an element of the horizontal plane (Zhdanov and Liu, 2013):

$$z = h(x,y) - H_0 = h^{(k)} - b_x^{(k)}(x - x_k) - b_y^{(k)}(y - y_k) - H_0 \tag{21}$$

and

$$b_x^{(k)}(x,y) = 0, \qquad b_y^{(k)}(x,y) = 0. \tag{22}$$

In such special cases, equation 19 can be represented as follows:

$$g_\alpha(\mathbf{r}_n') = \sum_{k=1}^{N_m} f_\alpha^{(nk)} h^{(k)}, \tag{23}$$

where

$$f_\alpha^{(nk)} = G[R(z_k) - R(-H_0)]\delta_{\alpha\eta} \frac{r_\eta^{(k)} - r_\eta^{(n)'}}{|\mathbf{r}^{(k)} - \mathbf{r}_n'|^3} \Delta x \Delta y, \tag{24}$$

where N_m is the number of cells and n is the index of the point of observation $\mathbf{r}_n'$.

We can obtain a similar formula for the gravity gradient fields:

$$g_{\alpha v}(\mathbf{r}_n') = \sum_{k=1}^{N_m} f_{\alpha v}^{(nk)} h^{(k)}, \tag{25}$$

where

$$f_{\alpha v}^{(nk)} = \frac{G[R(z_k) - R(-H_0)]\delta_{\alpha\eta}}{|\mathbf{r}^{(k)} - \mathbf{r}_n'|^5} [3(r_v^{(k)} - r_v^{(n)'})(r_\eta^{(k)} - r_\eta^{(n)'})$$

$$- |\mathbf{r}^{(k)} - \mathbf{r}_n'|^2 \delta_{v\eta}] \Delta x \Delta y. \tag{26}$$

We note that equations 23–26 may not be accurate enough for forward modeling because the accuracy of approximation by the piecewise horizontal surface may not be sufficient. However, these equations are very effective for calculating the Fréchet derivative

matrix in the inversion process because of their simplicity. More accurate numerical forms of the Cauchy-type integrals can be found in Zhdanov and Liu (2013).

INVERSION FOR A DENSITY CONTRAST SURFACE BASED ON 3D CAUCHY-TYPE INTEGRALS

In the previous sections, we discuss the forward modeling of gravity and gravity gradient fields based on 3D analogs of Cauchy-type integrals. In our forward modeling process, the model parameters were the elevations $h^{(k)} = h(x_k, y_k)$ of the density contrast surface with respect to the horizontal plane P, assuming the value of the density contrast is given. As we can see from the forward modeling equations, the forward operator is nonlinear. Correspondingly, the inversion is also a nonlinear problem. The traditional inversion of potential field data to find the density distribution is a linear problem, and the Fréchet derivative can be easily found and it does not change during the iterative inversion. In our inversion, the Fréchet derivative is a function of model parameters and may change from iteration to iteration.

Fortunately, in our inversion, the Fréchet derivative has an analytic form. In Appendices B and C, we derive the explicit expressions for the Fréchet derivative for the gravity and gravity gradient data.

As usual, the inversion of gravity and gravity gradient data is an ill-posed problem. To obtain stable and geologically reasonable result, we need to apply regularization to impose some restrictions on our solution. The inversion is based on the minimization of the Tikhonov parametric functional (Tikhonov and Arsenin, 1977):

$$P^\alpha(\mathbf{m}, \mathbf{d}) = (\mathbf{W}_d\mathbf{A}(\mathbf{m}) - \mathbf{W_d}\mathbf{d})^T(\mathbf{W}_d\mathbf{A}(\mathbf{m}) - \mathbf{W_d}\mathbf{d}) + (\mathbf{W}_m\mathbf{m} - \mathbf{W}_m\mathbf{m}_{\text{apr}})^T(\mathbf{W}_m\mathbf{m} - \mathbf{W}_m\mathbf{m}_{\text{apr}}), \quad (27)$$

where $\mathbf{A}$ is the forward modeling operator, $\mathbf{W}_d$ is the data weighting matrix, $\mathbf{d}$ is the vector of observed data, $\mathbf{m}$ is the vector of the model parameters $\mathbf{h}$, and $\mathbf{W}_m$ is a diagonal matrix of the model parameters weights based on integrated sensitivity:

$$\mathbf{W}_m = \mathbf{diag}(\mathbf{F}^T\mathbf{F})^{1/2}, \quad (28)$$

where $\mathbf{F}$ is the Fréchet derivative matrix.

The minimization problem 27 can be reformulated using a space of weighted parameters:

$$\mathbf{m}^w = \mathbf{W}_m\mathbf{m}. \quad (29)$$

In the weighted parameter's space, the Tikhonov parametric functional is given as follows:

$$P^\alpha(\mathbf{m}^w, \mathbf{d}) = (\mathbf{A}^w(\mathbf{m}^w) - \mathbf{d})^T(\mathbf{A}^w(\mathbf{m}^w) - \mathbf{d}) + \alpha(\mathbf{m}^w - \mathbf{m}^w_{\text{apr}})^T(\mathbf{m}^w - \mathbf{m}^w_{\text{apr}}), \quad (30)$$

where $\mathbf{A}^w$ is a new forward operator in the space of weighted parameters, which can be related to the forward operator $\mathbf{A}$ in the original space as

$$\mathbf{A}^w = \mathbf{A}\mathbf{W}_m^{-1}. \quad (31)$$

The minimization of the Tikhonov parametric functional is based on the reweighted regularized conjugate gradient method. With index $n + 1$ referring to the iteratively updated model n, the algorithm is given as follows (Zhdanov, 2002):

$$\mathbf{r}_n^w = \mathbf{A}^w(\mathbf{m}_n^w) - \mathbf{d} = \mathbf{A}(\mathbf{m}_n) - \mathbf{d}, \quad (32)$$

$$\mathbf{l}_{wn}^{\alpha_n} = \mathbf{F}_{wn}^T\mathbf{r}_n^w + \alpha_n(\mathbf{m}_n^{wn} - \mathbf{m}_{\text{apr}}^{wn}), \quad (33)$$

$$\beta_n^{\alpha_n} = \|\mathbf{l}_{wn}^{\alpha_n}\|^2/\|\mathbf{l}_{w(n-1)}^{\alpha_{n-1}}\|^2, \quad (34)$$

$$\widetilde{\mathbf{l}_{wn}^{\alpha_n}} = \mathbf{l}_{wn}^{\alpha_n} + \beta_n^{\alpha_n}\mathbf{l}_{w(n-1)}^{\alpha_{n-1}}, \qquad \widetilde{\mathbf{l}_{w0}^{\alpha_0}} = \mathbf{l}_{w0}^{\alpha_0}, \quad (35)$$

$$k_n^{\alpha_n} = (\widetilde{\mathbf{l}_{wn}^{\alpha_n}}^T\mathbf{l}_{wn}^{\alpha_n})/[\widetilde{\mathbf{l}_{wn}^{\alpha_n}}^T(\mathbf{F}_{wn}^T\mathbf{F}_{wn} + \alpha_n\mathbf{I})\widetilde{\mathbf{l}_{wn}^{\alpha_n}}], \quad (36)$$

$$\mathbf{m}_{n+1}^{w_n} = \mathbf{m}_n^{w_n} - k_n^{\alpha_n}\widetilde{\mathbf{l}_{wn}^{\alpha_n}}, \quad (37)$$

$$\mathbf{m}_{n+1} = \mathbf{W}_m^{-1}\mathbf{m}_{n+1}^{w_n}, \quad (38)$$

$$\mathbf{m}_{n+1}^{w_{n+1}} = \mathbf{W}_m\mathbf{m}_{n+1}, \quad (39)$$

$$\mathbf{s}_{n+1}^{w_{n+1}} = (\mathbf{m}_{n+1}^{w_{n+1}} - \mathbf{m}_{\text{apr}}^{w_{n+1}}), \qquad \mathbf{s}_{n+1}^{w_n} = (\mathbf{m}_{n+1}^{w_n} - \mathbf{m}_{\text{apr}}^{w_n}), \quad (40)$$

$$\gamma = \|\mathbf{s}_{n+1}^{w_{n+1}}\|^2/\|\mathbf{s}_{n+1}^{w_n}\|^2, \quad (41)$$

and

$$\alpha_{n+1} = \begin{cases} \alpha_n, & \gamma \le 1 \\ \alpha_n/\gamma, & \gamma > 1 \end{cases}. \quad (42)$$

We solve our problem in the space of the weighted model parameters. In the algorithm given above, $\mathbf{r}_n^w$ is a residual vector between the predicted and observed data; $\mathbf{l}_{wn}^{\alpha_n}$ is the steepest ascend direction; and $\widetilde{\mathbf{l}_{wn}^{\alpha_n}}$ is the conjugate gradient direction, which is a combination of the current steepest ascend direction and the previous conjugate gradient direction with the coefficient $\beta_n^{\alpha_n}$. We can see from equation 35 that the conjugate gradient direction is the same as the steepest ascend direction at the first iteration. The step length $k_n^{\alpha_n}$ is obtained using a linear line search scheme. The regularization parameter α_n is selected using an adaptive method as shown in our algorithm. Parameter $\mathbf{m}_{\text{apr}}^{w_n}$ represents an a priori model, selected based on all known information about the model parameters.

During the inversion process, the Fréchet derivative matrix changes in every iteration. One of the most expensive parts of inversion is the computation of the Fréchet derivative matrix. To speed up the inversion, the Fréchet derivative can be updated not on every iteration but after every five or 10 iterations.

We implement the developed theory and method in a computer code that is tested on several synthetic models as discussed below.

MODEL STUDIES

In this section, we present two model studies for the modeling and inversion of gravity data caused by density-contrast surface with a density contrast that is variable with the depth. In the first study, we consider a model of a sediment-basement interface with the density contrast varying linearly with the depth. Forward modeling based on the Cauchy-type integral method is compared with forward modeling based on the traditional method.

In the second case study, we assume a more complicated model with the density contrast between the sediment and basement changing exponentially with depth. We also apply the same inversion to the data simulated for the second model because a similar exponential density profile will be used for the inversion of the field data in the following section.

Model 1: Linear density variation

We assume that the density of the basement has a constant value of $\rho_b = 3000$ kg/m^3 and the density of the sediment at the surface is $\rho_0 = 2000$ kg/m^3 and it increases linearly with the depth according to the following formula:

$$\rho_s = \rho_0 + az, \tag{43}$$

where

$$\rho_0 = 2000 \text{ kg/m}^3, \qquad a = 5 \times 10^{-4} \text{ kg/m}^4. \tag{44}$$

We compare the forward modeling result obtained by the new method of Cauchy-type integrals with the result based on the traditional method, using volume integrals over the domain occupied by anomalous masses subdivided into the prismatic cells. The density inside each prismatic cell was set to be a constant. Figure 3 shows
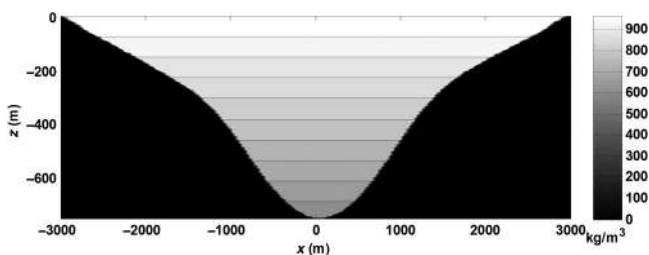
the representation of the density contrast distribution in model 1 using prismatic cells.

Gravity and vertical gravity gradient components were computed using these two methods. Figure 4 shows a comparison of forward modeling results obtained using the Cauchy-type integral and the traditional volume integral methods. We observe a very good fit between these results. A small difference can be attributed to the errors of the prismatic approximation of the volume density distribution in the traditional method and discretization of the surface for Cauchy-type integral calculation, respectively. We need to note that, for this model, the ratio of computation time required by the conventional method and by the Cauchy-type integral method is almost 30 on the same desktop PC.

Model 2: Exponential density variation

Model 2 has the same geometry of the depth-to-basement interface as model 1. However, the density contrast between sediment and basement varies exponentially with the depth according to the following expression:

$$\Delta\rho = ae^{-bz} + ce^{-dz}, \tag{45}$$

where

$$a = 251.5 \text{ kg/m}^3, \quad b = -0.007,$$
$$c = 197 \text{ kg/m}^3, \quad d = 5.2656 \times 10^{-6}. \tag{46}$$

Figure 5 shows the representation of the density contrast distribution in model 2 using prismatic cells. We present the gravity responses computed using Cauchy-type integral and the traditional volume integral methods in Figure 6. One can see that the result

Figure 3. Model 1. Representation of the density contrast distribution using prismatic cells.

Figure 5. A prism approximation of the density contrast surface with the density contrast changing exponentially with depth.
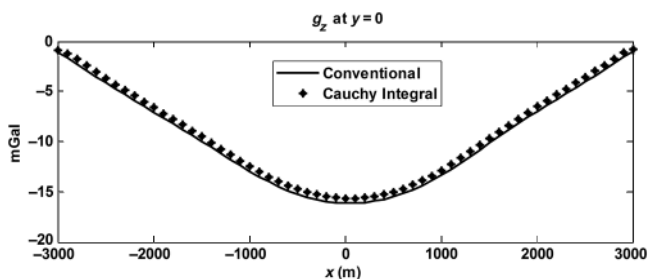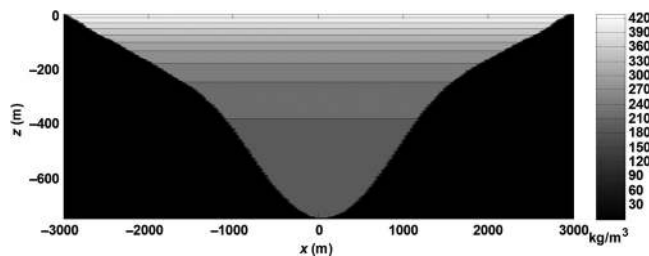

Figure 4. Model 1 — Comparison of forward modeling results obtained using Cauchy-type integral (dotted line) and traditional volume integral (solid line) methods.
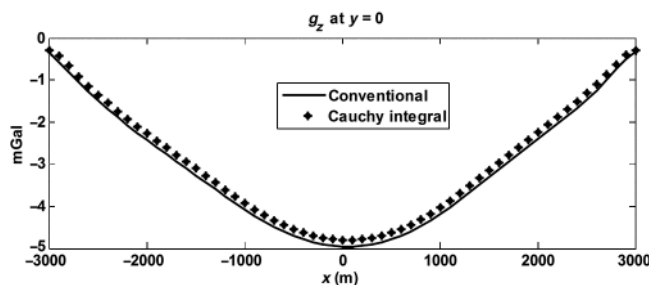

Figure 6. Model 2 — Comparison of forward modeling results obtained using Cauchy-type integral (dotted line) and traditional volume integral (solid line) methods.

produced by the new method practically coincides with that of the traditional method.

We apply the inversion algorithm introduced in the previous sections to the inversion of the synthetic data simulated for the model with exponential density variation.

Figure 7 shows the inversion result for the synthetic model with exponential density variation with depth. One can see that the density contrast surface was recovered well by this inversion.

INVERSION OF GRAVITY DATA AT THE BIG BEAR LAKE AREA

U.S. Geological Survey gravity survey at the Big Bear Lake area

Gravity surveys are widely used for basin study. The depth to basement can be well estimated based on isostatic Bouguer gravity data because the gravity anomaly is caused primarily by the density
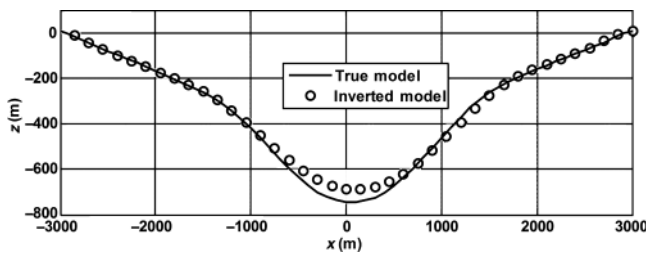
Figure 7. Inversion result for the model with the density contrast varying exponentially with depth.
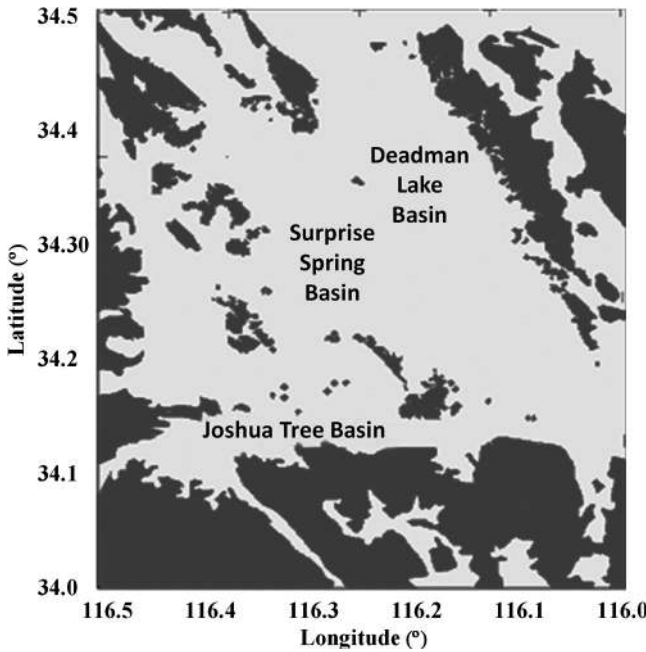
Figure 8. A USGS model of the basin for the Big Bear Lake area (Roberts et al., 2002). The dark zones indicate the location of outcrops.

contrast between the sediments and the basement. Many gravity measurements were made in the 1960s and 1970s by various groups to produce gravity maps covering California at a scale of 1:250,000 for the California Division of Mines and Geology (Roberts et al., 2002). The U.S. Geological Survey (USGS) also conducted a new gravity survey in the Big Bear Lake area. The new survey data were merged with the previous gravity survey to produce a new gravity grid (Roberts et al., 2002). We should note that in this paper we have gridded and used for the inversion only the data from the new USGS survey.

USGS applied the conventional prism inversion method to the combined new gravity data to recover the depth to basement. In their inversion, the subsurface was discretized to a grid of prisms, whose horizontal size was 2000×2000 m. The density distribution along each column of prisms was assumed to be known from the well-log data, and the thickness of the prisms was determined by fitting to the isostatic Bouguer gravity anomaly. The USGS inversion was well constrained by the well-log data and bedrock locations. In addition, at several locations, the thickness of the prisms was assumed to be known and stayed unchanged during the inversion (Roberts et al., 2002).

Due to a data ownership issue, USGS only released the new data they collected and the well-log data were not made available.

Geologic background of the Big Bear Lake area

The Big Bear Lake area is located in the southeast part of California. The area is characterized by a deep sedimentary basin surrounded by uplifted bedrock. USGS produced a basin model from the surface geology, well logs, and potential field data. Figure 8 shows that the whole basin area can be divided into three parts from the northeast to the southwest: the Deadman Lake, Surprise Spring, and Joshua Tree basins. The average depth and density variations between sediment and bedrock may be slightly different.

Figure 9 presents a digital elevation model (DEM) of the area. From the surface geology, we can observe three fault belts trending from the northwest to the southeast and one fault belt trending from
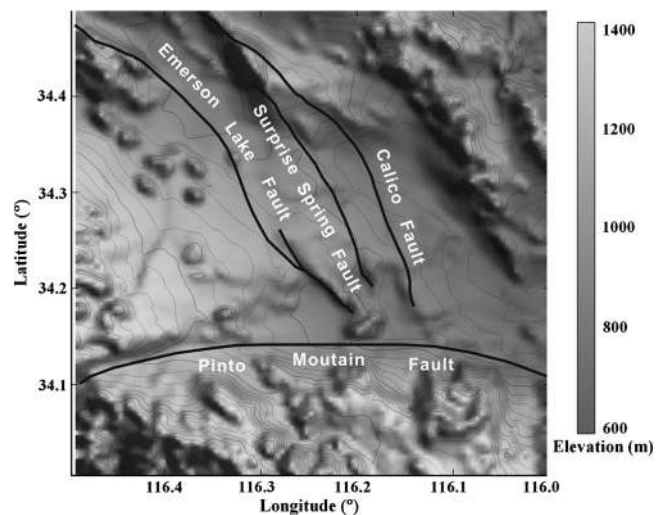

Figure 9. DEM of the Big Bear Lake area.

the west to the east. Different basins in this area are separated by these four main fault structures.

Processing of U.S. Geological Survey data

Figure 10 presents the released USGS data with the locations of the gravity stations shown by the black dots. As one can see, the original gravity data were collected in an irregular grid. It is well known that gridded data have a significant advantage over scattered data for inversion in terms of the robustness because having regular gridded data helps produce a robust inversion result. There are different gridding methods available. The traditional mathematical gridding approach can produce significant artifacts, especially in areas with a few observation stations. We use a gridding approach
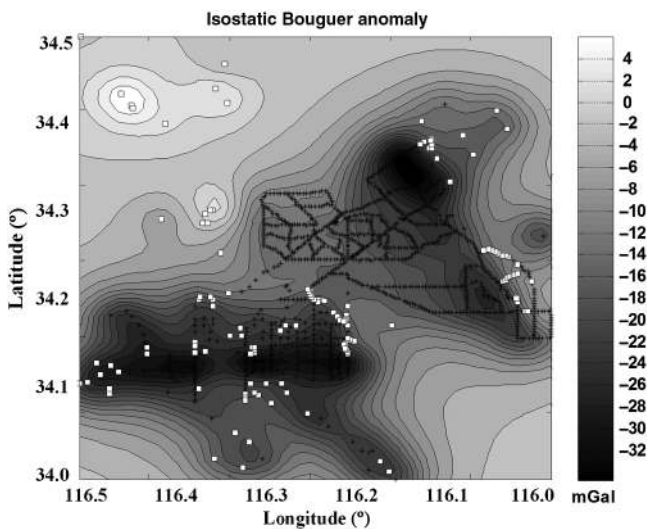
Figure 10. Gridded gravity data from the USGS survey. The black dots are the gravity stations, and the square markers denote the stations located on the bedrock.
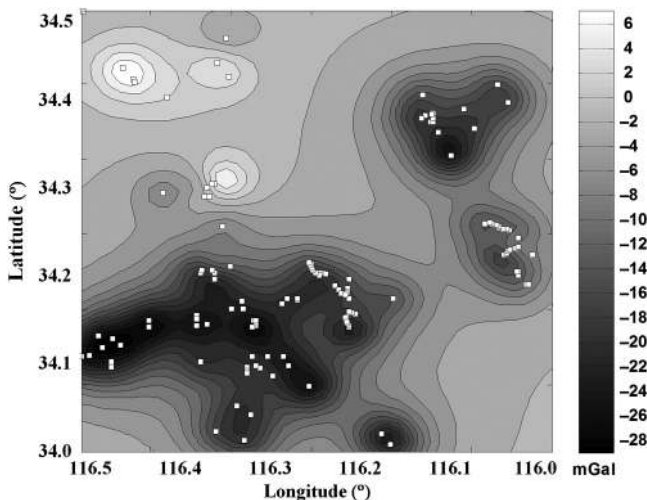

Figure 11. A gravity grid for the bedrock component of the isostatic Bouguer gravity anomaly. The square markers indicate the locations of the gravity stations on the outcrops.

based on the equivalent-source concept (Cordell, 1992). According to this concept, on the first step, we determine an equivalent layer with some surface density distribution recovered based on the inversion of the data collected in an irregular grid. On the next step, we compute the gravity data at the regular grid using the equivalent layer as the source.

Note that the gridded gravity data can be used directly for inversion if we assume that the isostatic Bouguer anomaly is caused purely by a deficiency in the density of the sediments. By making this assumption, we assume that the density of the bedrock is the same as in the reference density model of the earth's crust. However, in a real case, the density of the bedrock may be different from the reference model. Therefore, the isostatic Bouguer gravity anomaly can be written as a sum of the bedrock component and the sediment component as

$$g = g_b + g_s. \tag{47}$$

The bedrock gravity component g_b can be estimated initially based on the gravity data observed on the bedrock (Roberts et al., 2002). Figure 11 shows the gridded bedrock component. One can see that in the southern part, there is a strong negative anomaly for the bedrock gravity component. The gridded bedrock component of the gravity anomaly was subtracted from the gravity grid in Figure 10 to obtain the gravity anomaly caused by the sediment only. Figure 12 shows the gravity anomaly obtained after removal of the bedrock component. This grid represents the final data that we used for inversion.

We note that the approximation of the bedrock component of gravity anomaly by interpolating the anomaly observed on outcrops is not a rigorous approach due to the presence of a nearby sedimentary basin with low density. We use an iterative method to remove the bedrock gravity component. In our approach, the bedrock component of the gravity field is initially computed by simple extrapolation from the gravity observations on the bedrock outcrop. Inside the inversion, it is corrected based on the inverted basin depth. The corrections are terminated when there is no significant change in the bedrock component of the gravity field (Roberts et al., 2002).
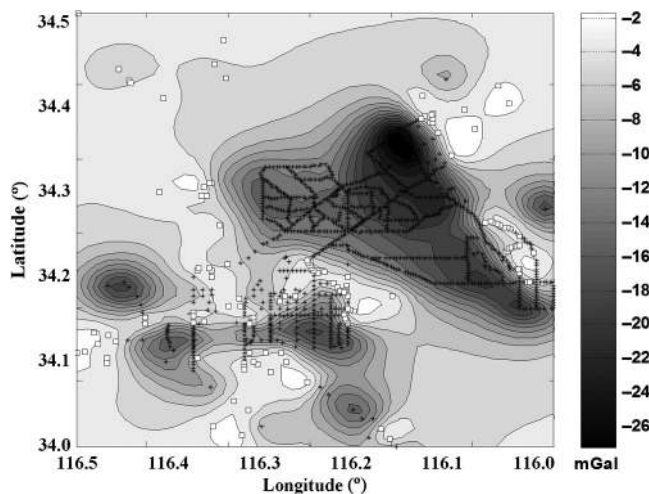

Figure 12. Isostatic Bouguer gravity grid after removal of the bedrock component.

Inversion of U.S. Geological Survey gravity data

One needs to know the density variation with the depth to get an accurate model of the depth to the basement. As we mentioned above, this information can be obtained from well-log data. The density models of the Deadman Lake and Surprise Spring basins are slightly different from that of the Joshua Tree basin. The USGS report states that in the northern part, a density contrast of 400, 350, 300, 250, and 200 kg/m³ with bottom depths of 50, 100, 150, and 300 m is a good approximation of the basin density (Roberts et al., 2002). The USGS report also states that this model may not be suitable for the Deadman Lake basin well because there are very limited well constraints in the Deadman Lake basin (Roberts et al., 2002). In the southern part (Joshua Tree basin), a constant density contrast value of 550 kg/m³ is suitable (Roberts et al., 2002). The northern part (the Deadman Lake and Surprise Spring basins) and the southern part (Joshua Tree basin) of the survey area will be inverted separately. To speed up the inversion and get the most reasonable result, the well-known Bouguer slab formula (Chakravarthi and Sundararajan, 2006) could be applied to generate an initial model:

$$z = \frac{g_B \Delta \rho_0}{41.89 \Delta \rho_0^2 + a g_B}, \quad (48)$$

where g_B is the Bouguer gravity anomaly and $\Delta \rho_0$ is the density contrast between the sediment and basement on the earth's surface and this density contrast decreases in the vertical direction with the gradient a.

However, our inversion algorithm does not depend on the selection of the starting model. The selection of a flat surface as a starting model produces almost the same result as using the Bouguer slab formula as a starting model.

In the inversion, we used a grid size of 300×300 m in the x- and y-directions, which is much finer than the USGS model grid for prismatic inversion (2000×2000 m).
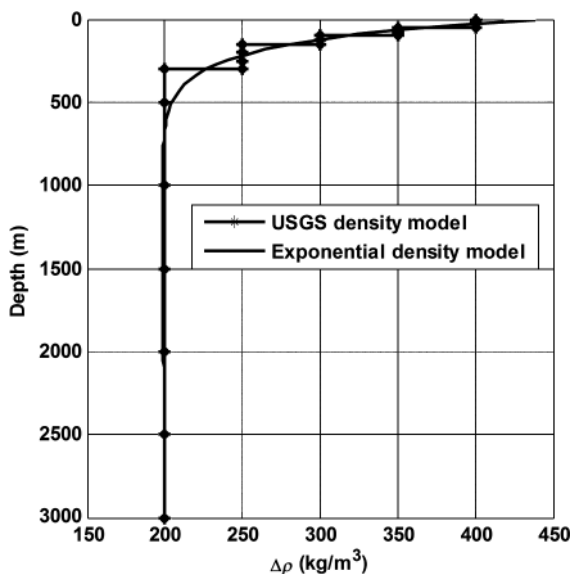

Figure 13. An approximation of the USGS staircase density variation model by the exponential function.

Inversion of gravity data in the Deadman Lake and Surprise Spring basins

To take the variable density contrast into account, we need to use some analytic function of depth to approximate the density contrast. For the USGS model, we found that it was better to use equation 45 to approximate the true density contrast. The optimized values for parameters in equation 45 are given in equation 46.

Figure 13 presents plots of the USGS staircase density variation model and our approximation by the exponential function. The results of the inversion are shown in Figure 14 overlapped with the DEM and the fault structure. One can see that the northwest–southeast-trending faults correspond well to the edge of Surprise Spring and Deadman Lake basins. The east edge of the recovered Deadman Lake basin fits well with the mountain belt. Figure 15 shows an overlap of the inversion result with the USGS basin and bedrock models. In this figure, one can see that the recovered location of the basin is similar to the USGS model.

Figure 16 shows a comparison of our inversion result with the inversion result provided by USGS for the Deadman Lake and Surprise Spring basins. One can see that the recovered basin geometry obtained by our method correlates well with the USGS model. However, the recovered maximum depths are slightly different (4500 m for the USGS inversion result). The USGS report mentioned that the recovered depth of the basement for the Deadman
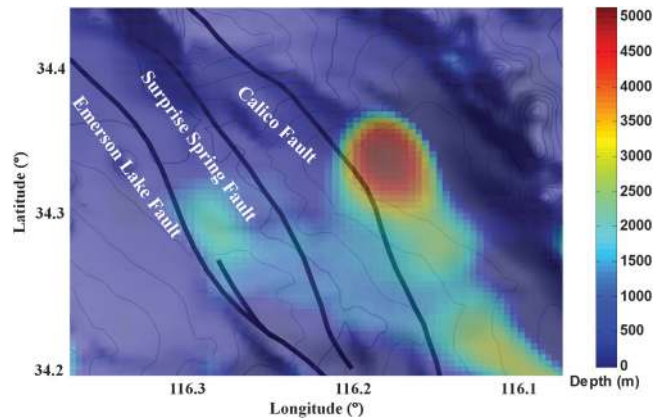

Figure 14. Results of the inversion of the gravity data for the Deadman Lake and Surprise Spring basins overlapped with the DEM map indicated by the gray background with isolines.
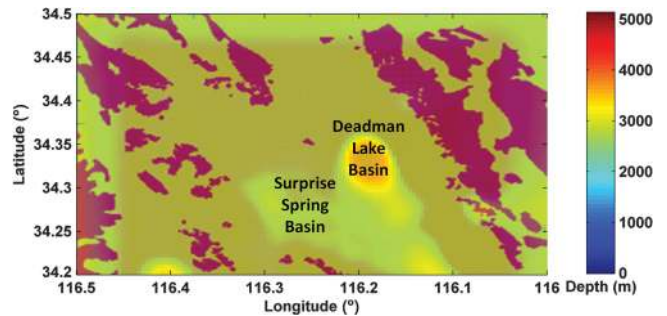

Figure 15. Results of the inversion of the gravity data for the Deadman Lake and Surprise Spring basins overlapped with the USGS model of the outcrops and sediment basin.

Lake basin in their inversion may be underestimated due to the absence of the well-log data (Roberts et al., 2002).

Figure 17 shows a comparison of the observed and predicted data. The final normalized misfit was 10%, and the convergence became flat after 20 iterations. This tolerance was a reasonable
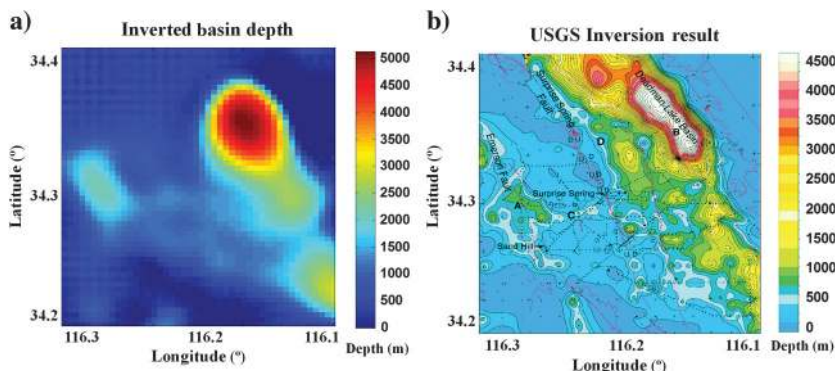
number considering the noise level of the real data. However, we ran our inversion with a constant density contrast of 300, 400, and 500 kg/m³, and all of these inversions provided much better data fitting with the final normalized misfit being less than 5%. Based on these results, we conclude that the USGS density model for the Deadman Lake and Surprise Spring basins may not be optimal.

Inversion of gravity data in the Joshua Tree basin

For the inversion of the gravity data in the Joshua Tree basin, the USGS used several different density models. They found that a constant density contrast of 550 kg/m³ is a good approximation of the true density distribution (Roberts et al., 2002). We used the same value in our inversion.

Figure 18 shows our inversion results overlapped with the DEM and fault structure. One can see that the edges of the inverse gravity model of the basin correspond well to the Pinto Mountain belt. Figure 19 presents our inversion results overlapped with the USGS density model of the basin and bedrock models. We can see in this figure that the recovered location of the basin is very similar to the USGS model. The recovered depth is close to zero on the bedrock.

Figure 20 shows a comparison of our inversion results with the inversion result provided by USGS for the Joshua Tree basin. One

Figure 16. Panel (a) shows the inverted basin depth for the Deadman Lake and Surprise Spring basins, and panel (b) is the inversion result produced by USGS (after Roberts et al., 2002).
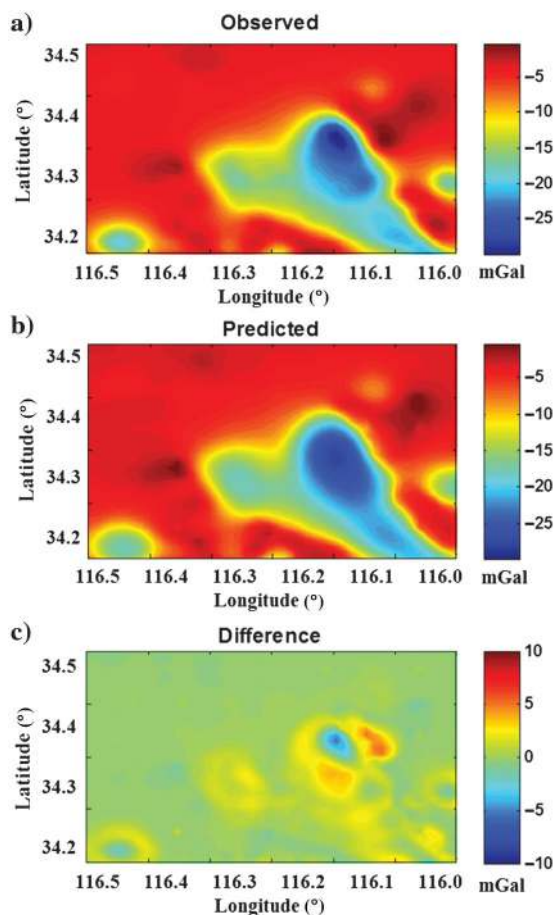

Figure 17. A comparison of the (a) observed and (b) predicted data for the inversions of the gravity data in the Deadman Lake and Surprise Spring basins. Panel (c) shows the difference between the observed and predicted data.
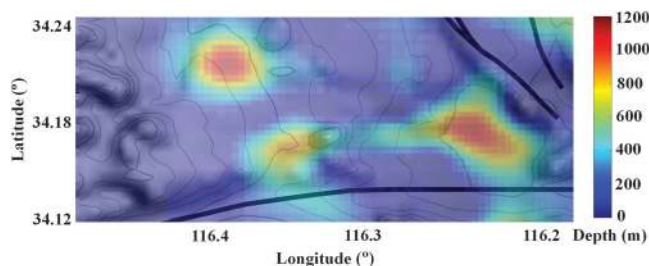

Figure 18. Results of the inversion of the gravity data in the Joshua Tree basin overlapped with the DEM map indicated by the gray background with isolines.
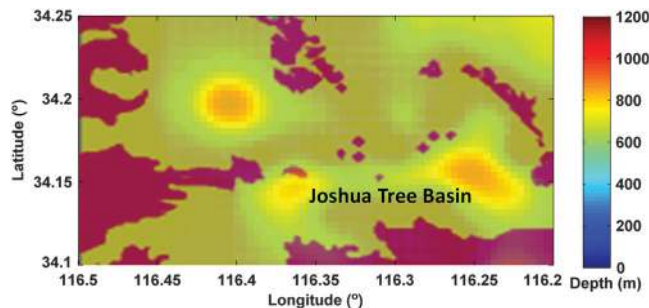

Figure 19. The results of the inversion of the gravity data for the Joshua Tree basin overlapped with the USGS model of the outcrops and sediment basin.

can see that the basin geometry recovered using our method correlates well with the USGS model. The maximum depth determined by our inversion is also in a good agreement with the USGS model (1100 m for the USGS inversion result).

Figure 21 presents a comparison between the observed and predicted data. The final normalized misfit was 5%, and it took only five iterations to reach the given misfit level.

CONCLUSIONS

We have developed a new method for modeling gravity data caused by a sediment-basement interface with a variable density contrast distribution in the vertical direction. Our method is based on the Cauchy-type integral approach, which reduces the volume integration to the surface integration.

We validate our forward-modeling algorithm for linear and exponential density contrast distributions with depth by comparing our result with conventional prism-based modeling. Based on the forward modeling, we also develop an inversion algorithm to recover the depth to basement for the models with variable density contrast with depth. The inversion is tested on a synthetic model of the basin with an exponential density contrast distribution. We demonstrate with the synthetic models that the depth to basement can be recovered well.

We also apply our method for inversion of the field data collected by the USGS in the Big Bear Lake area. The recovered basin shape and depth correspond well to the results produced by the USGS and to the known geology.

In conclusion, we would like to emphasize that using surface Cauchy-type integrals reduces the computational expenses significantly in comparison with the conventional volume integral methods. The developed approach to interpretation of the gravity data for the study of basins makes it practical to invert gravity data on a large scale while using very fine discretization of the sediment-basement interface.

ACKNOWLEDGMENTS

APPENDIX A

A 3D ANALOG OF THE CAUCHY-TYPE INTEGRAL AND ITS PROPERTIES

A 3D analog of the Cauchy-type integral and its derivation is introduced by Zhdanov (1988) as follows:

Figure 21. A comparison of the (a) observed and (b) predicted gravity data for the inversions in the Joshua Tree basin. Panel (c) shows the difference between the observed and predicted data.
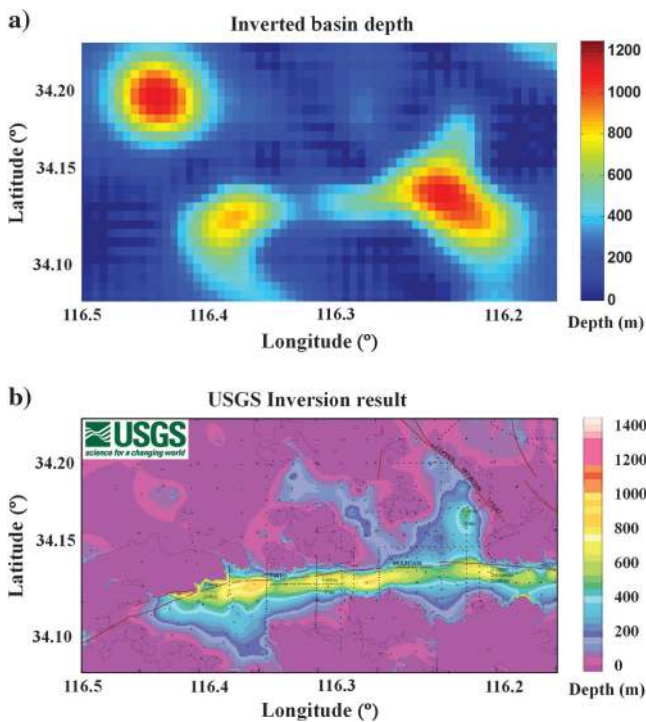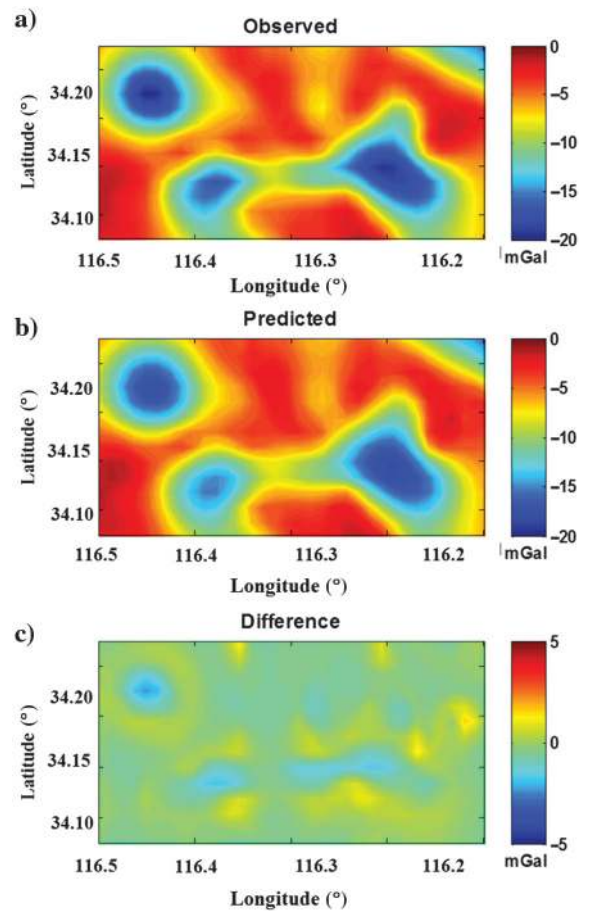

Figure 20. Panel (a) shows the inverted basin depth for the Joshua Tree basin, and panel (b) is the inversion result produced by USGS (after Roberts et al., 2002).

$$\mathbf{C}^s(\mathbf{r}', \boldsymbol{\varphi}) = \frac{-1}{4\pi} \int \int_S \left[(\mathbf{n} \times \boldsymbol{\varphi}) \nabla \frac{1}{|\mathbf{r} - \mathbf{r}'|} + (\mathbf{n} \times \boldsymbol{\varphi}) \right.$$
$$\left. \times \nabla \frac{1}{|\mathbf{r} - \mathbf{r}'|} \right] \mathrm{d}s, \tag{A-1}$$

where S is some closed surface bounding a domain D; $\boldsymbol{\varphi} = \boldsymbol{\varphi}(\mathbf{r})$ is some vector function defined on the closed surface S; and $\mathbf{n}$ is the normal vector to the surface S, pointing outside D. The vector function $\mathbf{C}^s$ is called the vector density of the Cauchy-type integral. It is demonstrated by Zhdanov (1988) that everywhere outside of S, the vector function $\mathbf{C}^s$ represents the Laplace vector field, which satisfies the following equations:

$$\nabla \cdot \mathbf{C}^s = 0, \qquad \nabla \times \mathbf{C}^s = 0. \tag{A-2}$$

Thus, the scalar components of vector function $\mathbf{C}^s$ are harmonic functions. In a special case where $\boldsymbol{\varphi}(\mathbf{r})$ stands for the boundary values on S of the gradient of a function harmonic inside domain D, a 3D Cauchy-type integral can be calculated using the following formula:

$$\mathbf{C}^s(\mathbf{r}', \boldsymbol{\varphi}) = \begin{cases} \boldsymbol{\varphi}(\mathbf{r}'), & \mathbf{r}' \in D \\ \mathbf{0}, & \mathbf{r}' \in CD \end{cases}, \tag{A-3}$$

where CD is a complement of the closed domain D with respect to the whole space.

It is shown by Zhdanov (1988) that one can formulate a 3D analog of the Pompei formula for the Cauchy-type integral, which is given by the following expression:

$$\mathbf{C}^s(\mathbf{r}', \mathbf{f}(\mathbf{r})) + \frac{1}{4\pi} \int \int \int_D (\nabla \times \mathbf{f}) \nabla \frac{1}{|\mathbf{r} - \mathbf{r}'|} \mathrm{d}v$$
$$= \begin{cases} \mathbf{f}(\mathbf{r}'), & \mathbf{r}' \in D \\ \mathbf{0}, & \mathbf{r}' \in CD \end{cases}, \tag{A-4}$$

where vector field $\mathbf{f}$ is an arbitrary potential field that satisfies the following equations:

$$\nabla \times \mathbf{f} = q, \qquad \nabla \times \mathbf{f} = 0. \tag{A-5}$$

In equation A-5, we consider q as a general source, and it takes the value of $-4\pi G\rho$ for the gravity problem.

In a special case where $\mathbf{f}$ is a Laplace field in D, equation A-4 reduces to a 3D Cauchy integral formula that is given in equation A-1.

The Cauchy-type integral formulas can be represented using matrix notations. The matrix form makes them suitable for numerical computation, which is important in practical applications. We take the convention that the z-axis is directed upward. In a Cartesian coordinate system $\{\mathbf{d}_x, \mathbf{d}_y, \mathbf{d}_z\}$, we can represent the vectors $\mathbf{C}^s, \boldsymbol{\varphi}, \mathbf{n}$, and $\nabla \frac{1}{|\mathbf{r} - \mathbf{r}'|}$ as follows:

$$\mathbf{C}^s = \mathbf{C}_\alpha^s \mathbf{d}_\alpha, \quad \boldsymbol{\varphi} = \varphi_\beta \mathbf{d}_\beta, \quad \mathbf{n} = n_\gamma \mathbf{d}_\gamma, \tag{A-6}$$

and

$$\nabla \frac{1}{|\mathbf{r} - \mathbf{r}'|} = -\frac{r_\eta - r_\eta'}{|\mathbf{r} - \mathbf{r}'|^3} \mathbf{d}_\eta, \tag{A-7}$$

where $r_\eta = \eta$; $\alpha, \beta, \gamma, \eta = x, y, z$, and we also use the convention that the twice recurring index indicates a summation over the index. Using these notations, we can write the scalar components of the Cauchy-type integral as follows:

$$\mathbf{C}_\alpha^s = \frac{-1}{4\pi} \int \int_S \Delta_{\alpha\beta\gamma\eta} \varphi_\beta \frac{r_\eta - r_\eta'}{|\mathbf{r} - \mathbf{r}'|^3} n_\gamma \mathrm{d}s,$$
$$\alpha, \beta, \gamma, \eta = x, y, z, \tag{A-8}$$

where the four-index Δ-symbol is expressed in terms of the symmetric Kronecker symbol $\delta_{\alpha\beta}$ as

$$\Delta_{\alpha\beta\gamma\eta} = \delta_{\alpha\beta}\delta_{\gamma\eta} + \delta_{\alpha\eta}\delta_{\beta\gamma} - \delta_{\alpha\gamma}\delta_{\beta\eta}; \delta_{\alpha\beta} == \begin{cases} 1, & \alpha = \beta \\ 0, & \alpha \neq \beta \end{cases}. \tag{A-9}$$

APPENDIX B

FRÉCHET DERIVATIVE CALCULATION FOR A GRAVITY AND GRAVITY GRADIENT OPERATORS FOR A DENSITY CONTRAST MODEL WITH CONSTANT DENSITY CONTRAST

For simplicity, we approximate the density contrast surface with a piecewise horizontal surface as we have shown in equations 23–26.

We will start with the vertical component of the gravity field:

$$g_z(\mathbf{r}_n') = \sum_{k=1}^{N_m} f_z^{(nk)} h^{(k)}, \tag{B-1}$$

where

$$f_z^{(nk)} = -G\gamma\rho_0 \frac{z^{(k)} - z^{(n)'}}{|\mathbf{r}^{(k)} - \mathbf{r}_n'|^3} \Delta x \Delta y$$
$$= -G\rho_0 \frac{h^{(k)} - H_0 - z^{(n)'}}{|\mathbf{r}^{(k)} - \mathbf{r}_n'|^3} \Delta x \Delta y. \tag{B-2}$$

The matrix of the Fréchet derivative can be found by direct differentiation of the forward-modeling equation B-1 as follows:

$$F_{nl} = \frac{\partial g_z(\mathbf{r}_n')}{\partial h^{(l)}} = \frac{\partial \sum_{k=1}^{N_m} f_z^{(nk)} h^{(k)}}{\partial h^{(l)}}$$
$$= \sum_{k=1}^{N_m} \left[\frac{\partial f_z^{(nk)}}{\partial h^{(l)}} h^{(k)} + f_z^{(nk)} \frac{\partial h^{(k)}}{\partial h^{(l)}} \right]. \tag{B-3}$$

We note that

$$\frac{\partial h^{(k)}}{\partial h^{(l)}} = \delta_{kl}, \tag{B-4}$$

and

$$\frac{\partial f_z^{(nk)}}{\partial h^{(l)}} = -G\rho_0 \Delta x \Delta y \frac{\partial}{\partial h^{(l)}} \left[\frac{h^{(k)} - H_0 - z^{(n)'}}{|\mathbf{r}^{(k)} - \mathbf{r}_n'|^3} \right]$$

$$= G\rho_0 \Delta x \Delta y \left[3\frac{(h^{(l)} - H_0 - z^{(n)'})^2}{|\mathbf{r}^{(l)} - \mathbf{r}_n'|^5} - \frac{1}{|\mathbf{r}^{(l)} - \mathbf{r}_n'|^3} \right]. \quad \text{(B-5)}$$

By substituting equations B-4 and B-5 into equation B-3 and applying some algebra, we finally arrive at the solution for the Fréchet derivative matrix as follows:

$$F_{nl} = \frac{G\rho_0 \Delta x \Delta y}{|\mathbf{r}^{(l)} - \mathbf{r}_n'|^3} \left\{ \frac{3(h^{(l)} - H_0 - z^{(n)'})^2}{|\mathbf{r}^{(l)} - \mathbf{r}_n'|^2} h^{(l)} \right.$$

$$\left. - (2h^{(l)} - H_0 - z^{(n)'}) \right\}. \quad \text{(B-6)}$$

The derivation of the Fréchet derivative matrix for gravity gradient data is very similar to that of vertical gravity component, but more complicated math will be involved. Still, we use the piecewise horizontal surface to approximate the density contrast surface within each cell. By taking the derivative of equation 25 with respect to $h^{(l)}$, after reduction, we arrive at the solution for the Fréchet derivative matrix for gravity gradiometry as shown in the following equation:

$$F_{\alpha v}^{(nl)} = \frac{G\rho_0 \Delta x \Delta y h^{(l)}}{|\mathbf{r}^{(l)} - \mathbf{r}_n'|^5} [3\delta_{zv}(r_\alpha^{(l)} - r_\alpha^{(n)'}) + 3\delta_{z\alpha}(r_v^{(l)} - r_v^{(n)'})$$

$$+ 2\delta_{v\alpha}(h^{(l)} - H_0 - z^{(n)'})]$$

$$+ \frac{G\rho_0 \Delta x \Delta y p_{\alpha v}^{(nl)}}{|\mathbf{r}^{(l)} - \mathbf{r}_n'|^5} \left(1 - 5h^{(l)} \frac{(h^{(l)} - H_0 - z^{(n)'})}{|\mathbf{r}^{(l)} - \mathbf{r}_n'|^2} \right). \quad \text{(B-7)}$$

APPENDIX C

FRÉCHET DERIVATIVE CALCULATION FOR GRAVITY AND GRAVITY GRADIENT OPERATORS FOR DENSITY CONTRAST MODEL WITH VARIABLE DENSITY CONTRAST

For a model with variable density contrast $\Delta\rho(z)$, the gravity field can be written in the matrix form as follows:

$$g_z(\mathbf{r}_n') = \sum_{k=1}^{N_m} f_z^{(nk)} [R(-H_0) - R(z_k)], \quad \text{(C-1)}$$

where the kernel is defined by the following equation:

$$f_z^{(nk)} = G\frac{(h^{(k)} - H_0 - z^{(n)'})}{|\mathbf{r}^{(k)} - \mathbf{r}_n'|^3} \Delta x \Delta y. \quad \text{(C-2)}$$

In the last equation, we use the following notations:

$$R(\mathbf{z}) = \int_{-H_0}^{z} \Delta\rho(z) dz. \quad \text{(C-3)}$$

The matrix of the Fréchet derivative can be found by direct differentiation of the forward-modeling operator C-1 as follows:

$$F_{nl} = \frac{\partial g_z(\mathbf{r}_n')}{\partial h^{(l)}} = \frac{\partial \sum_{k=1}^{N_m} f_z^{(nk)}}{\partial h^{(l)}} = \sum_{k=1}^{N_m} \left[\frac{\partial f_z^{(nk)}}{\partial h^{(l)}} \right]. \quad \text{(C-4)}$$

We note that

$$\frac{\partial h^{(k)}}{\partial h^{(l)}} = \delta_{kl}. \quad \text{(C-5)}$$

After some algebra, we can find an analytic expression for the Fréchet derivative in a discretized form as follows:

$$F_{nl} = \frac{G[R(h^{(l)} - H_0) - R(-H_0)]}{|\mathbf{r}^{(l)} - \mathbf{r}_n'|^3}$$

$$\times \left[3\frac{(h^{(l)} - H_0 - z^{(n)'})^2}{|\mathbf{r}^{(l)} - \mathbf{r}_n'|^2} - 1 \right] \Delta x \Delta y$$

$$- G\Delta\rho(h^{(l)}) \frac{(h^{(l)} - H_0 - z^{(n)'})}{|\mathbf{r}^{(l)} - \mathbf{r}_n'|^3} \Delta x \Delta y. \quad \text{(C-6)}$$

The derivation of the Fréchet derivative matrix for gravity gradient data is also very similar to that of vertical gravity component, but more complicated math will be involved. Here, we will show the expression of the Fréchet derivative matrix for gravity gradient data in the case of variable density distribution without the details of derivation:

$$F_{\alpha v}^{(nl)} = G\Delta\rho(h^{(l)})\delta_{\alpha\eta}A\Delta x \Delta y$$

$$+ G[R(h^{(l)} - H_0) - R(-H_0)]\delta_{\alpha\eta}B\Delta x \Delta y, \quad \text{(C-7)}$$

where

$$A = \frac{3(r_v^{(l)} - r_v^{(n)'})(r_\eta^{(l)} - r_\eta^{(n)'}) - |\mathbf{r}^{(l)} - \mathbf{r}_n'|^2 \delta_{v\eta}}{|\mathbf{r}^{(l)} - \mathbf{r}_n'|^5} \quad \text{(C-8)}$$

and

$$B = \frac{[5|\mathbf{r}^{(l)} - \mathbf{r}_n'|^2 \delta_{v\eta} - 15(r_v^{(l)} - r_v^{(n)'})(r_\eta^{(l)} - r_\eta^{(n)'})](h^{(l)} - H_0 - z^{(n)'})}{|\mathbf{r}^{(l)} - \mathbf{r}_n'|^7}$$

$$+ \frac{3\delta_{z\eta}\delta_{zv} - 2(h^{(l)} - H_0 - z^{(n)'})\delta_{v\eta}}{|\mathbf{r}^{(l)} - \mathbf{r}_n'|^5}. \quad \text{(C-9)}$$

REFERENCES

Barbosa, V., J. Silva, and W. Medeiros, 1997, Gravity inversion of basement relief using approximate equality constraints on depths: Geophysics, **62**, 1745–1757, doi: 10.1190/1.1444275.

Barbosa, V., J. Silva, and W. Medeiros, 1999a, Gravity inversion of a discontinuous relief stabilized by weighted smoothness constraints on depth: Geophysics, **64**, 1429–1437, doi: 10.1190/1.1444647.

Barbosa, V., J. Silva, and W. Medeiros, 1999b, Stable inversion of gravity anomalies of sedimentary basins with nonsmooth basement reliefs and arbitrary density contrast variations: Geophysics, **64**, 754–764, doi: 10.1190/1.1444585.

Cai, H., and M. S. Zhdanov, 2015, Modeling and inversion of magnetic anomalies caused by sediment–basement interface using three-dimensional Cauchy-type integrals: IEEE Geoscience and Remote Sensing Letters, **12**, 477–481, doi: 10.1109/LGRS.2014.2347275.

Chakravarthi, V., and N. Sundararajan, 2006, Gravity anomalies of 2.5-D multiple prismatic structures with variable density: A Marquardt inver-

sion: Pure and Applied Geophysics, **163**, 229–242, doi: 10.1007/s00024-005-0008-8.

Chávez, R. E., O. Lazaro-Mancilla, J. O. Campos-Enríquez, and E. L. Flores-Márquez, 1999, Basement topography of the Mexicali Valley from spectral and ideal body analysis of gravity data: Journal of South American Earth Sciences, **12**, 579–587, doi: 10.1016/S0895-9811(99)00041-3.

Cordell, L. E., 1992, A scattered equivalent-source methods for interpolation and gridding of potential-field data in three dimensions: Geophysics, **57**, 629–636, doi: 10.1190/1.1443275.

Gallardo-Delgado, L., M. Pérez-Flores, and E. Gómez-Treviño, 2003, A versatile algorithm for joint 3D inversion of gravity and magnetic data: Geophysics, **68**, 949–959, doi: 10.1190/1.1581067.

LaFehr, T. R., and M. N. Nabighian, 2012, Fundamentals of gravity exploration: SEG.

Martins, C., V. Barbosa, and J. Silva, 2010, Simultaneous 3D depth-to-basement and density-contrast estimates using gravity data and depth control at few points: Geophysics, **75**, no. 3, I21–I28, doi: 10.1190/1.3380225.

Martins, C., W. Lima, V. Barbosa, and J. Silva, 2011a, Total variation regularization for depth-to-basement estimate: Part 1 — Mathematical details and applications: Geophysics, **76**, no. 1, I1–I12, doi: 10.1190/1.3524286.

Martins, C., W. Lima, V. Barbosa, and J. Silva, 2011b, Total variation regularization for depth-to-basement estimate: Part 2 — Physicogeologic meaning and comparisons with previous inversion methods: Geophysics, **76**, no. 1, I13–I20, doi: 10.1190/1.3524286.

Odegard, M. E., 2011, A sediment thickness map of South America using automated inversion of magnetic and gravity data for depth to basement: 12th International Congress of the Brazilian Geophysical Society and EX-POGEF, SEG and Brazilian Geophysical Society, 581–586.

Roberts, C., R. Jachens, A. Katzenstein, G. Smith, and R. Johnson, 2002, Gravity map and data of the eastern half of the Big Bear Lake, 100,000 scale quadrangle, California and analysis of the depths of several basins: U.S. Geological Survey, Open-file report 02-353.

Silva, J., D. Costa, and V. Barbosa, 2006, Gravity inversion of basement relief and estimation of density contrast variation with depth: Geophysics, **71**, no. 5, J51–J58, doi: 10.1190/1.2236383.

Silva, J., W. Medeiros, and V. Barbosa, 2001, Potential field inversion: Choosing the appropriate technique to solve a geologic problem: Geophysics, **66**, 511–520, doi: 10.1190/1.1444941.

Silva, J., A. Oliveira, and V. Barbosa, 2010a, Gravity inversion of 2D basement relief using entropic regularization: Geophysics, **75**, no. 3, I29–I35, doi: 10.1190/1.3374358.

Silva, J., F. Oliveira, V. Barbosa, and H. Campos Velho, 2007, Apparent-density mapping using entropic regularization: Geophysics, **72**, no. 4, I51–I60, doi: 10.1190/1.2732557.

Silva, J., S. Vasconcelos, and V. Barbosa, 2010b, Apparent-magnetization mapping using entropic regularization: Geophysics, **75**, no. 2, L39–L50, doi: 10.1190/1.3358160.

Tikhonov, A. N., and V. Y. Arsenin, 1977, Solutions of ill-posed problems: V. H. Winston & Sons.

Zhdanov, M. S., 1980, Use of Cauchy integral analogs in the geopotential field theory: Annales de Geophysique, **36**, 447–458.

Zhdanov, M. S., 1984, Cauchy integral analogs in geophysical field theory (in Russian): Nauka.

Zhdanov, M. S., 1988, Integral transforms in geophysics: Springer-Verlag.

Zhdanov, M. S., 2002, Geophysical inverse theory and regularization problems: Elsevier.

Zhdanov, M. S., and H. Cai, 2013, Inversion of gravity and gravity gradiometry data for density contrast surfaces using Cauchy-type integrals: 83rd Annual International Meeting, SEG, Expanded Abstracts, 1161–1165.

Zhdanov, M. S., and X. Liu, 2013, 3-D Cauchy-type integrals for terrain correction of gravity and gravity gradiometry data: Geophysical Journal International, **194**, 249–268, doi: 10.1093/gji/ggt120.